Research paper

Variability of the surface properties of sepiolite

M. Suárez [a,*], E. García-Romero [b,c]

[a] Área de Cristalografía y Mineralogía, Departamento de Geología, Universidad de Salamanca, Plaza de la Merced s/n, E-37008, Salamanca, Spain
[b] Departamento de Cristalografía y Mineralogía, Facultad de Geología, Universidad Complutense de Madrid, Avd. José Antonio Novais s/n, E-28040, Madrid
[c] Instituto de Geociencias, (Universidad Complutense de Madrid—Consejo Superior de Investigaciones Científicas) Avd. José Antonio Novais E-28040, Madrid

Keywords:
Sepiolite
Specific surface area
BET
Microporosity
Texture
Electron microscopy

A B S T R A C T

A comparative study of a wide collection of sepiolites (22 samples from different locations, including samples coming from the greatest deposits of sepiolite in the world) was made with the aim of understanding the real variability of the surface properties in sepiolite. The samples have been studied by XRD, Electron Microscopy (TEM and SEM) and the adsorption–desorption of N_2. The influence of possible impurities, crystallinity and crystalline defects, and the textural variations, is taken into account to explain the high differences found in the specific surface area of sepiolites. The studied samples display a high variability in crystallinity, fibre length and texture. The BET surface varies between 77 and 399 $m^2 g^{-1}$, demonstrating the significant variation in the surface properties in natural sepiolites. Both the external and the microporous area vary between very wide extreme values, from 52 $m^2 g^{-1}$ to 246 $m^2 g^{-1}$ for the microporous area and 6 $m^2 g^{-1}$ to 178 $m^2 g^{-1}$ for the external area. The exceptionally low values of these properties found in some samples cannot be related to the presence of impurities, but rather to their structural and textural features. Two types of microporosity that can be described are *structural microporosity* and *interfibre microporosity*. The SSA and the porosity of each sepiolite is the result of the sum of the intracrystalline or structural microporosity and the textural porosity (interfibre microporosity and mesoporosity). As a consequence, there is a hierarchical distribution of pore sizes, which is different for each sepiolite. The lowest values of microporosity are related to the presence of very open pores and the sepiolites with higher SSA are those having a smaller length and a more closed porosity.

1. Introduction

Sepiolite is a clay mineral with a wide range of industrial applications based on its physicochemical properties, especially its surface properties. Exhaustive reviews of the industrial uses of sepiolite are given in Murray (1999), Álvarez et al. (2011) and Ruiz Hitzky et al. (2011). Industrial uses of sepiolite are related to its sorptive, colloidal–rheological and catalytic properties. Some examples are the adsorption of cationic-, anionic- and neutral surfactants (Özdemir et al., 2007; del Hoyo et al., 2008) and the preparation of a wide variety of nanocomposites (Gómez-Avilés et al., 2010; Jia et al., 2010; Chen et al., 2011) as well as a variety of others. More recently, the use of sepiolite in health care products (Viseras et al., 2008) and in the geological storage of CO_2 (Galán et al., 2011) has been investigated.

Sepiolite is a mineral with fibrous morphology due to its crystalline structure. The structure of this mineral was described by Brauner and Presinger (1956) as continuous sheets of tetrahedral silica that have an apical oxygen periodically inverted. This periodical inversion produces each three tetrahedral chains in the [001] direction. The tetrahedral sheets are bound to octahedral sheets, which are discontinuous in the [010] direction, and continuous and elongated in the [001] direction. The nature of the octahedral sheets is fully magnesic although isomorphic substitutions are possible and Al and Fe^{3+} can also appear (Garcia-Romero and Suarez, 2010). The Mg cations that occupy the most external positions in the octahedral sheets complete their coordination spheres with two molecules of water, named coordinated water. The discontinuity of the octahedral sheet, due to the periodical inversion of an apical oxygen in the tetrahedral sheet, produces structural channels that run parallel to the c axis of the crystal and, consequently, to the fibre. These intracrystalline channels offer a great surface that can be accessible, or partially accessible, to different molecules (Inagaki et al., 1990). In the last years, *channel* has been used to describe refer the surface of the crystal, because one face is open, and *tunnel* has been used to describe the intra-crystalline voids. The tunnels have cross section of about 4×11 $Å^2$ and hold zeolitic water. This zeolitic water is easily released by heating over 150 °C or under vacuum at rt (Post et al., 2007; Rautureau and Mifsud, 1977). Half of the coordinated water is released when sepiolite is heated over 350 °C forming a new semi-anhydrous phase in a process named *folding* (Serna et al., 1975; Frost and Ding, 2003 and Post et al., 2007 among others). Channels and tunnels of folded sepiolite change in shape and size after folding

(Rautureau and Mifsud, 1977). The possibility of the existence of intergrowths between sepiolite and palygorskite has been recently proposed (Chryssikos et al., 2009; Stathopoulou et al., 2011 and Suárez and García-Romero, 2011). In that case, the existence of ribbons like palygorskite in the inside of the crystal of sepiolites could produce a lower structural microporosity.

Sepiolite can have high specific surface area (SSA) values not only as a result of the small size of its particles, but also because of its fibrous morphology and its intra-crystalline tunnels. Both the external surface and the surface of the micropores influence the SSA of this mineral. The most common method to studying the SSA of porous solids is the BET method (Brunauer et al., 1936). The reported values of the BET surface area for sepiolite range between ~80 and 350 m^2/g^{-1} (Nishimura et al., 1972), although recently Alvarez has reported the surface area for sepiolite to be 320 m^2g^{-1} (Álvarez et al., 2011). After reports by Shuali et al. (2011), representative values of the measured surface areas are 230–320 m^2g^{-1}. Theoretical values of the external surface (~400 m^2g^{-1}) and the internal surface (500 m^2g^{-1}) were calculated by Serna and Van Scoyoc (1979) for sepiolite from Vallecas (Spain). Sepiolite from Vallecas is probably the most studied sepiolite from the point of view of its physicochemical properties. The measured values of SSA are far from the calculated theoretical values, even when molecules smaller than N_2 are used as sorbate. Based on a study by Dandy and Nadiye-Tabbiruka (1982), monolayers of N_2 molecules on all internal surfaces are unlikely to formed. The N_2 accessibility to the intra-crystalline tunnels is restricted both by the relative size of N_2 and the tunnels, and by the presence of the zeolitic water filling the tunnels. The intra-pore adsorption of small and short-branched molecules like pyridine and acetone does occur (Kuang et al., 2006). To measure the internal surface area due to the tunnels, the release the zeolitic water without dehydrating coordinated water is necessary. Several studies have been done investigating the best out-gassing conditions of sepiolite (Balci, 1999; Campelo et al., 1987, among others) and they agreed that a very mild heating of the sample under vacuum is necessary to eliminate zeolitic water. This treatment increases the SSA obtained as compared to the measurements obtained without heating the sample. The processes of out-gassing that are generally employed (under vacuum and ~100 °C for several hours) allow the release the zeolitic water without achieving structure folding. When sepiolite suffers a pre-treatment of heating over 300 °C under vacuum the SSA measurement obtained was decreased (Balci, 1999 and Campelo et al., 1987), however, these studies do not take the process of folding into account. Ruiz Hitzky (2001) showed that the structural microporosity disappears by crystal folding after a pre-treatment of sepiolite at 350 °C under dynamic vacuum was performed to eliminate the coordinated water molecules. According to Shuali et al. (2011) "the porosity spectrum of sepiolite or palygorskite is attributed to the contribution of two sources: a) External porosity resulting from the inter-fibres/bundles spaces and b) Structural porosity resulting from the repeated inversion of the silicate layer."

Other physical pre-treatments of the samples, like grinding, can also influence the SSA, in the two ways, increasing or decreasing the specific surface area. Cornejo and Hermosín (1988) demonstrated that a very soft grinding of sepiolite from Vallecas increased its BET surface and a more intense grinding produced the contrary effect, decreasing its BET surface, due to a partial amorphization of the mineral.

Sepiolite is a mineral which can have different crystalline defects, variable size, and different ways of aggregation of the fibres. These variations are the result of the growth conditions and they depend on the genetic environment (hydrothermal and sedimentary, mainly) and the processes involved (neoformation, transformation or mechanical heritage). The crystallochemical and textural characteristics of the mineral influence on its surface and explain the very wide different values of SSA reported in the literature, in addition to the different methodologies and pre-treatments employed. This last point is nontrivial, because very different results can be obtained by studying not only samples from the same locality but also from the same sample like the Sep-sp-1 sepiolite (supplied by the Clay Repository).

The importance of understanding the surface properties of sepiolite is important for numerous industrial applications. However, the inconsistencies found in the literature describing these surface properties are a result of not only the utilization of different processes for the pretreatment and analysis of these materials, but also from the expected differences for samples obtained from different geological origins. The aim of our work is to make a comparative study of a wide collection of sepiolites utilizing uniform laboratory and data analysis procedures. To the best of our knowledge, this is the first time that such a broad and comparative study has been described. This systematic study will aim to elucidate the true variability of the surface properties in sepiolite and the influence from variables like crystallinity and texture on these properties.

2. Materials and methods

Sepiolites from different sources and geological origins were sought to perform this study. 22 samples of sepiolite (Table 1) from different locations were studied, including samples coming from the greatest deposits of sepiolite in the world, like Vallecas-Vicálcaro (Spain), Polatli-Eskisehir (Turkey) and Nevada (USA). The samples were classified by taking their textural characteristics in hand sample into account. Therefore, samples were split into two groups: 1) Macroscopics, consisting of fibres of several millimetres to centimetres in length (Fig. 1), which can be seen by the naked eye or using a lens and 2) Clays: with an earthy aspect and the size of a grain which cannot be seen by optical microscopy. Table 1 contains the classifications, locations of provenance, and the labels used in this work. Some of these samples have been recently studied by HRXRD and microdiffraction with synchrotron radiation (Sánchez del Río, et al., 2011).

Mineralogical characterization was performed by X-ray diffraction (XRD) using a Siemens D500 XRD diffractometer with Cu Kα radiation and a graphite monochromator. The samples used were

Table 1
List of the sepiolite samples, including type, labeling, origin, approximated purity (from XRD data) and found impurities. The minerals in brackets appear as traces.

Type	Label	Procedence	% Sepiolite	Impurities (traces)
Macroscopic sepiolites	CER	Cerro Mercado (Mexico)	100	–
	FIN	Finland	60	Talc
	HEN	Henan (China)	100	(Talc)
	NEI	Neixiang (China)	95	Calcite
	NOR	Norwey	~100	
	XIX	Xixia (China)	~100	(Quartz)
Clay sepiolites	BAT	Cerro Batallones (Spain)	100	–
	GRA	Grant County (U.S.A.)	100	–
	HUN	Hunan (China)	70	Quartz, Talc
	MAR	Mara (Spain)	~100	(Smectite)
	MER	Eiskisehir (Turkey)	100	–
	MON	Monferrato (Italy)	100	–
	NAM	Namibia	85	Calcite
	NEV	Nevada (U.S.A.)	90	Quartz, (Feldspar)
	PEC	Pecharromán (Spain)	95	Quartz, Dolomite, (Palygorskite)
	POL	Polatli (Turkey)	85	Quartz, Dolomite, (Palygorskite)
	SAN	Santa Cruz (U.S.A.)	80	Calcite
	SOM	Somalia	70	Quartz, (Palygorskite)
	TPO	Polatli (Turkey)	95	Dolomite
	VAL	Vallecas (Spain)	~100	(Quartz)
	VIC	Vicálvaro (Spain)	100	–
	YUN	Yunclillos (Spain)	100	–

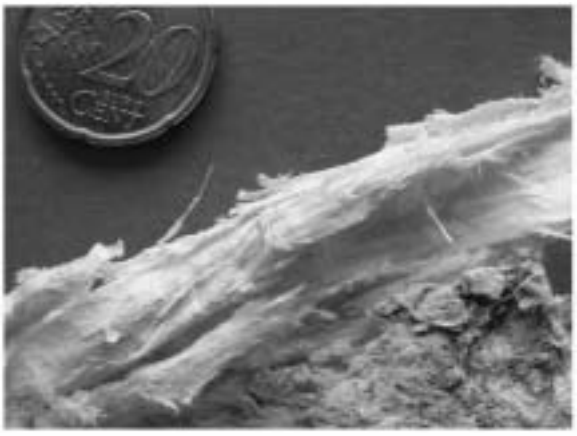

Fig. 1. Hand-sample of the macroscopic sepiolite from Henan (China) with fibres or bundles of fibres of centimetres in length.

random-powder specimens. They were powdered by hand in an agate mortar and the powders were scanned from 2 to 65° 2θ at a 0.05° 2θ/3 s scan speed to determine the purity of the samples. Semi-quantitative analysis of the crystalline phase was made following the methods of Schultz (1964).

The particle morphology and textural relationships were established by scanning electron microscopy using both, scanning- (SEM and FEG) and transmission electron microscopy (TEM) techniques. SEM observations were performed using a JEOL JSM 6400 microscope, operating at 20 kV, and FEG observations were carried out with a JEOL JSM-6330 F (Field Emission Scanning Electron Microscope) operating at 10 kV, wd 15 mm and SEI. Prior to SEM-FEG examinations, freshly fractured surfaces of representative samples were air-dried and coated with Au under vacuum. TEM observations were performed by depositing a drop of the diluted suspension on a microscopic grid with collodion. Images were obtained using a JEOL 2000 FX microscope equipped with a double-tilt sample holder (up to a maximum of ±45°) at an acceleration voltage of 200 kV, with a 0.5 mm zeta-axis displacement and 0.31 nm point-to-point resolution.

Textural analyses were carried out from the corresponding N_2 adsorption–desorption isotherms at −196 °C, obtained from a static-volumetric apparatus (Micromeritics ASAP 2010 adsorption analyzer). All samples were pre-treated and analysed in the same way: 0.3 g of the raw sample, powdered in a manual mortar, were outgassed for 2 h at rt and then 4 h at 110 °C at a reduced pressure of 2 μm Hg. The isotherms were obtained following a previously fixed 40-points P/P_0 table and the reproducibility of isotherms was checked.

3. Results

The samples studied were found to be pure or almost pure in most cases. Fig. 2 shows the XRD patterns of the purest sepiolites. Table 1 contains the mineralogical composition including the main impurities found in some samples and the amount of sepiolite estimated by semi-quantitative analysis from XRD. Quartz, carbonates (calcite, magnesite or dolomite) and talc are the main impurities observed in some of the sepiolite samples. Palygorskite also appears as an impurity in SOM, BOS and PEC samples in trace amounts. Notably, the coexistence of the two fibrous clay minerals, sepiolite and palygorskite, is not frequent in nature (García-Romero et al., 2007).

All XRD patterns of the studied samples present the reflections of sepiolite, but a detailed study of these patterns allows us to find some differences. These differences are related to both the position and the width of the peaks. As can be seen in Table 2, the position of the main reflection of sepiolite, corresponding to the (110) plane, varies between 11.986 Å and 12.253 Å for NEI and MER samples, respectively.

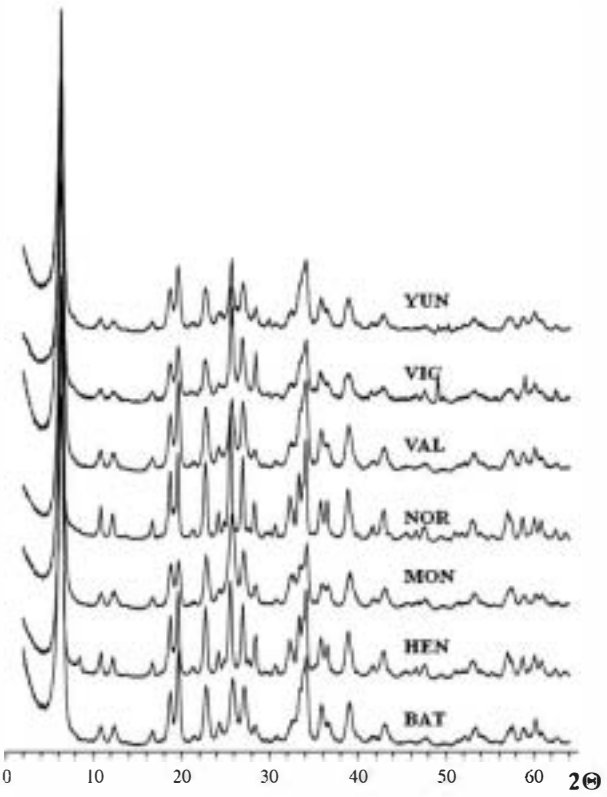

Fig. 2. XRD patterns of some of the purest sepiolites studied.

Sánchez del Río et al. (2011) also found differences in the d-spacing of the 110 reflection in the study of sepiolite with high resolution XRD, and they attributed the important changes observed to modifications in the cell originated by compositional variations caused by isomorphic substitutions. The differences in the width of this and the other peaks are even bigger than the differences in the position. The values of the FHWM (full width at half maximum) for this peak, described in Table 2, range from 0.3812° 2Ø for the NOR sample, the most crystalline sepiolite studied, and 1.3769° 2Ø for the MER sample. Although most macroscopic sepiolites are among the most crystalline samples (<0.6 FHWM), GRA and XIX samples are the two exceptions. GRA is a clay sepiolite and has one of the lower values of the FHWM parameter, indicating very good crystallinity, and XIX sample is a macroscopic sepiolite and its FHWM value is close to 0.9.

The textural features observed by electron microscopy, both transmission (TEM) and scanning (SEM-FEG), confirm that all of the samples studied present the characteristic fibrous morphology and can be seen in Figs. 3 and 4. Nevertheless, a more detailed study allows us to realise that the samples from different deposits have their own textural features. Although the samples can be differentially classified

Table 2
Parameters from X-ray powder diffraction: d-spacing and FWHM (in deg) of the 110 peak.

Sample	d_{110}(Å)	FHWM (110)	Sample	d_{110}(Å)	FHWM (110)
BAT	12.056	0.6931	NEV	12.12	0.9554
CER	12.038	0.5486	NOR	12.059	0.3812
FIN	12.059	0.4669	PEC	12.074	0.8549
GRA	12.051	0.5327	POL	12.16	0.831
HEN	12.023	0.4408	SAN	12.018	1.1162
HUN	12.121	0.7091	SOM	12.082	0.7117
MAR	12.1	0.7305	TPO	12.183	0.7965
MER	12.253	1.3769	VAL	12.104	0.6559
MON	12.005	0.6867	VIC	12.112	0.687
NAM	12.153	0.716	XIX	12.125	0.8743
NEI	11.968	0.5721	YUN	12.115	0.7008

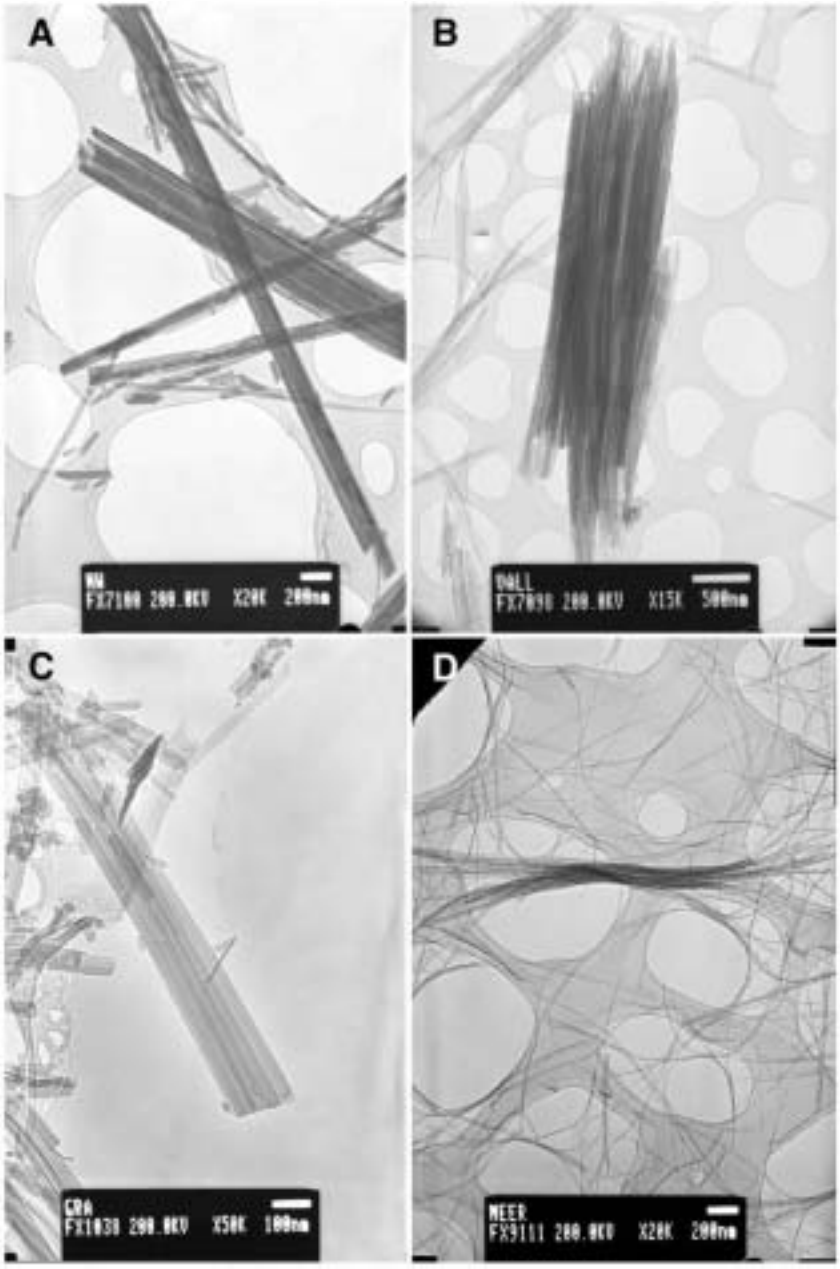

Fig. 3. TEM images of bundles of sepiolite fibres from different localities. A: MER (Eskisehir, Turkey), B: NOR (Norwey), C: SOM (Somalia), and D: VAL (Vallecas, Spain). The width of the "unit fibres" is similar and it does not depend on the length of the fibres. A, C, and D are clay sepiolites, while B is macroscopic.

as macroscopic and clay sepiolites depending on the length of the fibres, all of them are nanometric in size with respect to the cross section of the fibres, as can be seen in Figs. 3 and 4. Although the minimal width of the constituting fibres, as observed by electron microscopy, is always the same ("unit fibre"), the way each fibre gathers together to form bigger fibres (characteristic of each sample) varies. Usually, "unit fibres" group in arrangements with all the long axes approximately parallel, forming thicker fibres with "cylindrical" appearances (Fig. 4-A). Fibres commonly flock into groups of a few of these arranged in parallel to define the tape-like shapes. Very often, fibres form flat tablets which are made up of parallel or tangled fibres. The differences previously enumerated can result in different sizes, different curls, or different types of fibre aggregation as shown in Fig. 4. Fibres can show lengths of less than 1 μm (Fig. 4-C and D), like the sepiolite obtained from Nevada which has small fibres (shorter than 1 μm), to centimetres (macroscopic, Figs. 1, 4-A and B). However, sepiolites from some of the Spanish (Mara) or Turkish (Polatly and Meerschaunm) deposits consist of intermediate fibres (between 1 and 10 μm of length, Fig. 4-E and F). The Spanish deposits of sepiolite from Vicálvaro and Vallecas are formed by long fibres (longer than 10 μm). In addition, irrespective of their size, the fibres can show an extended range of bending or curling. For example, the completely straight and rigid fibres or slightly curly fibres like the samples from the Spanish deposits from Vallecas vary greatly from the very curly fibres like the samples from Meerschaum. The fibre width also varies among deposits and sometimes a direct correlation with the fibre length cannot be established. As a consequence, different porosities arise from the combinations of different characteristics. Sepiolite can therefore occur as either grown out fibres with the fibres resembling sticks (open porosity, Fig. 4-B and F), or as dense fibre masses, connected to each other forming a dense mesh (closed porosity, Fig. 4-C and D).

The isotherms of adsorption desorption of N_2 are similar for all of the studied samples (Fig. 5). They can be classified as Type II of the IUPAC classification which does not present a limited adsorption at

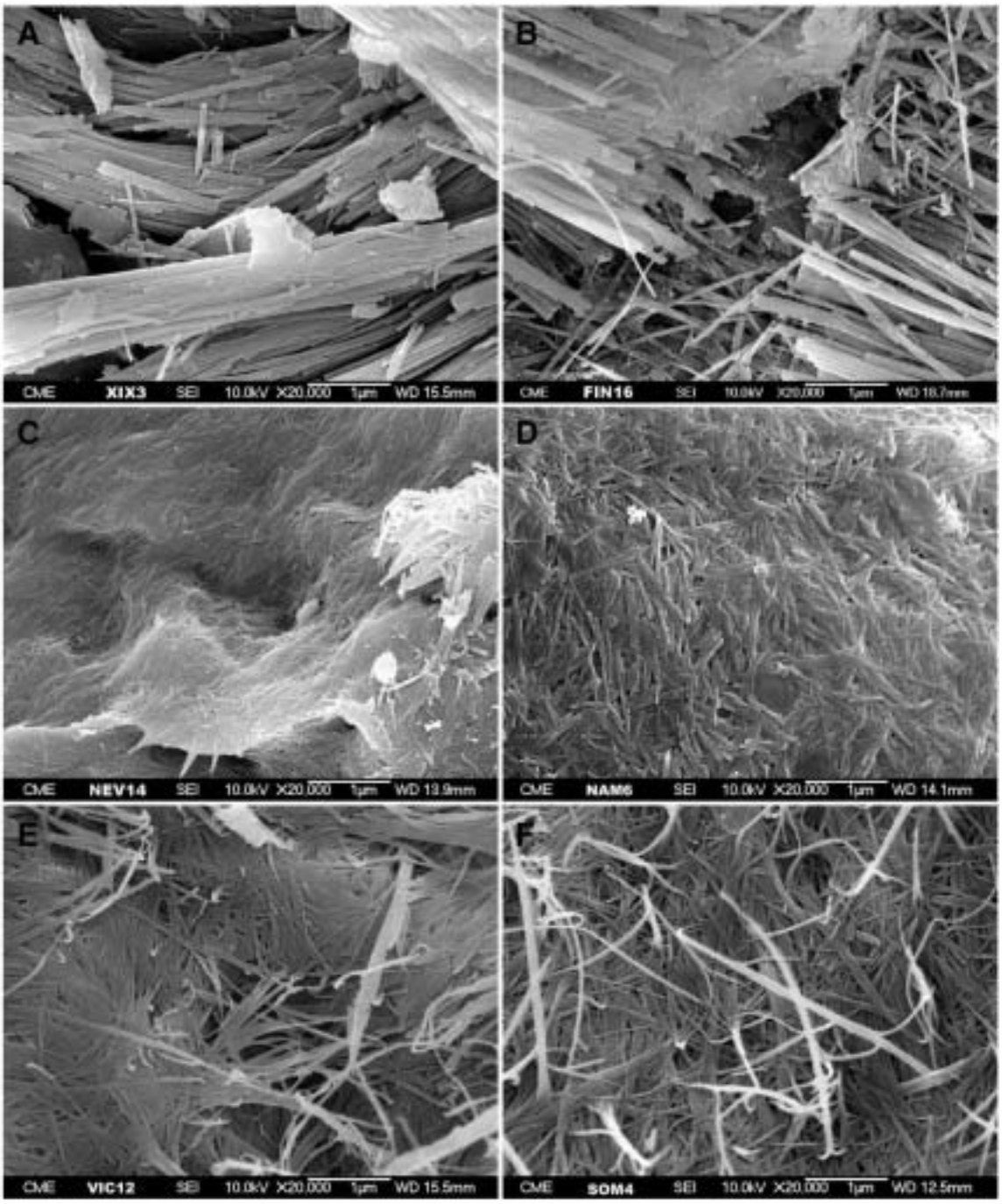

Fig. 4. FEG images of sepiolites from different localities. A: XIX (Xixia, China), B: FIN (Finland), C: NEV (Nevada, U.S.A.), D: NAM (Namivia), E: VIC (Vicalvaro, Spain), and F: SOM (Somalia). The size (length and width) and textural features of samples are very different. A and B are macroscopic, straight and rigid fibres. C and D are very short fibres and have very closed porosity. E and F are intermediate in size and show very curly fibres. B and F have very open porosity. Note that all the images have the same magnification.

relative pressures close to the unit. Most samples present a high adsorption at the lowest relative pressures as corresponding to the microporous solids (samples MER and BAT in Fig. 5). All of the samples present very small hysteresis loops corresponding to Type A, which indicates the presence of tubular pores (de Boer and Lippens, 1964). Only SAN sample (Fig. 5) presents hysteresis with a small loop type B of the same classification indicating the presence of pores formed by parallel plates. The values of the BET surface, the external surface, the microporous area and the volume appear in Table 3. The SSA of the samples is very different and ranges between 77 and 399 $m^2\,g^{-1}$ for XIX and MER samples, respectively. The sample with the greatest microporosity is BAT, and the lowest microporosity corresponds to GRA sample.

4. Discussion

The sepiolites investigated in this study are very different from the point of view of their crystallinity, texture, porosity and SSA. The SSA ranges between ~75 m^2g^{-1} and ~400 m^2g^{-1}; demonstrating that there is a significant difference in the surface properties of this mineral. Sepiolite is widely used as adsorbent material and its sorptive and catalytic properties are studied in different ways in hundreds of papers. In a wide, but not exhaustive, review of the literature concerning these aspects in the past several years, the variation in the value of the SSA (BET surface) elucidated ranges between 83 m^2g^{-1} and 350 m^2g^{-1}, for sepiolites from Turkey (Güngör et al., 2006 and Türker et al., 1997, respectively). The sepiolites more frequently

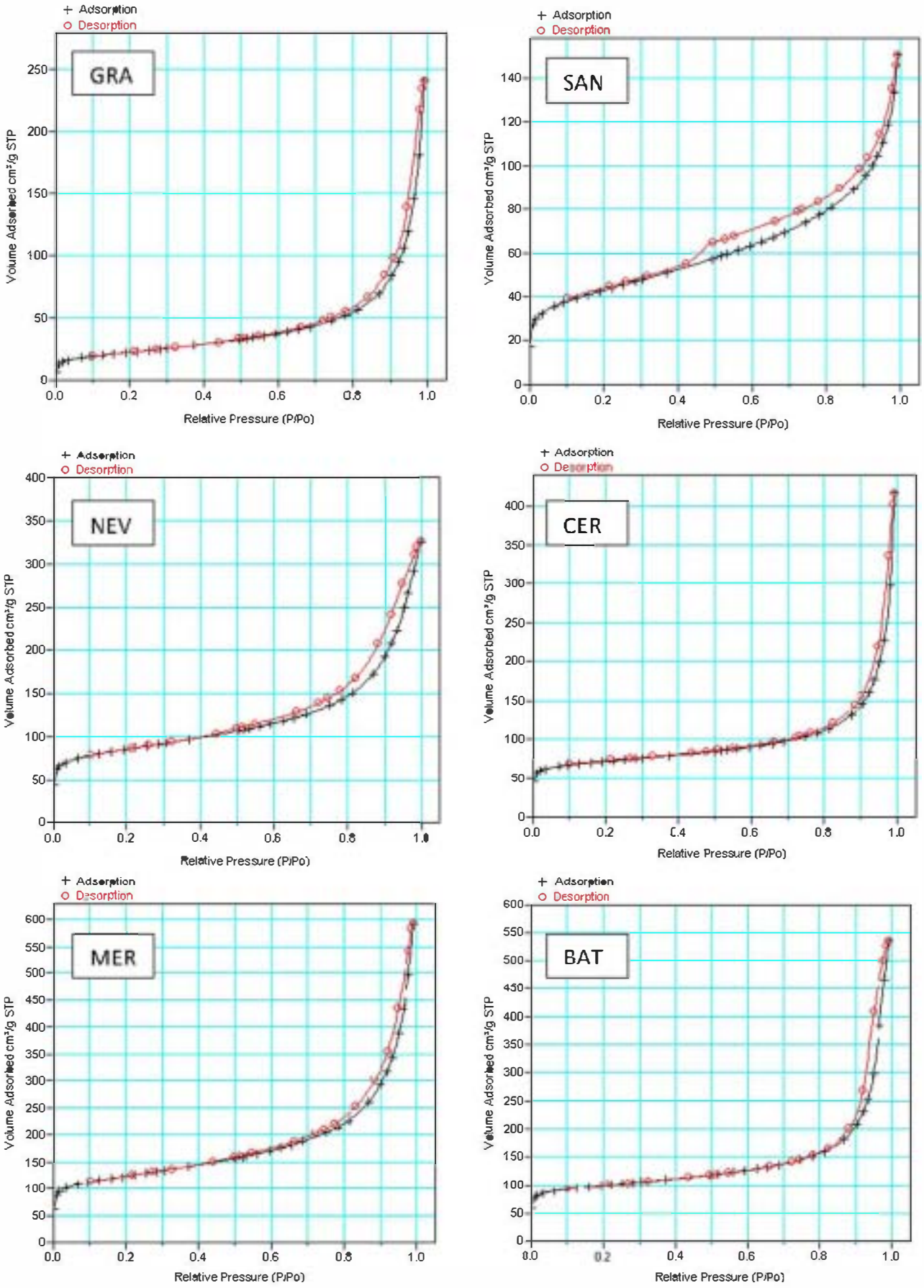

Fig. 5. Adsorption–desorption isotherms of N_2 of some representative samples.

Table 3
Data from the N_2 adsorption desorption isotherms. SSA_{BET}: Specific surface area from BET equation. SSA_{Ext} External specific surface area obtained from the t-method. $SSA_{\mu p}$: microporous area obtained from the t-method. $V_{\mu p}$ t: volume of microporous obtained from the t-method. V_{mp}BJH: Specific mesopore volume from Barrett–Joyner–Halenda method. Samples indicated with * have different amounts of impurities.

Sample	SSA_{BET} (m^2g^{-1})	SSA_{Ext} (m^2g^{-1})	$SSA_{\mu p}$ (m^2g^{-1})	$V_{\mu p}$ t (cm^3g^{-1})	V_{mp}BJH (cm^3g^{-1})
BAT	322	144	178	0.0920	0.759
CER	190	80	110	0.0678	0.568
FIN*	97	56	41	0.0214	0.237
GRA	79	73	6	0.0030	0.408
HEN	186	59	127	0.0628	0.3
HUN*	120	74	46	0.0243	0.506
MAR	268	150	118	0.0628	0.488
MER	399	246	153	0.0832	0.867
MON	229	135	94	0.0515	0.456
NAM*	196	100	96	0.0112	0.095
NEI	149	87	62	0.0316	0.363
NEV*	274	162	112	0.0618	0.466
NOR	120	57	63	0.0354	0.310
PEC*	225	133	92	0.0475	0.405
POL*	202	160	42	0.0208	0.896
SAN*	146	115	32	0.0163	0.226
SOM*	227	120	106	0.0437	0.404
TPO	239	142	97	0.0573	0.526
VAL	308	157	151	0.0887	0.563
VIC	217	120	97	0.0513	0.453
XIX	77	52	25	0.0197	0.242
YUN	295	151	144	0.0860	0.428

used in these studies come from the deposits from Eskisehir and Polatli (Turkey) and Vallecas (Spain). Samples from these deposits were also studied in this work. The data for the BET surface of sepiolite from Eskisehir ranges between 243 m^2g^{-1} (Mehmet, 2009) and 342 m^2g^{-1} (Alkan et al., 2007), although the most frequent value observed is ~330 m^2g^{-1}. The sepiolite from Eskisehir (MER) has a BET surface of ~400 m^2g^{-1}. For sepiolites from the deposit of Polatli, a high variability in the results described in the literature has also been found, and the BET values range between 163 m^2g^{-1} and 269 m^2g^{-1}. These extreme values correspond to two varieties, beige and brown, after Ünal and Erdogan (1998). Our sepiolite from Polatli (TPO sample) has a value of 239 m^2g^{-1}. Sepiolite from Hunan (China) has been studied recently by Zheng et al. (2010), both before and after acid and aluminium modification. This sepiolite has a BET surface of 110 m^2g^{-1}, which is close to the value of 120 m^2g^{-1} that we observed studying sepiolite from the same area (here named HUN).

The biggest deposit of sepiolite is Vallecas-Vicalvaro (Spain) and samples coming from this deposit are the most widely used in studies of the physicochemical properties of this mineral. Data of SSA reported for this sepiolite range between 189 m^2g^{-1}, found by Sánchez-Martín et al. (2006) and 340 m^2/g^{-1} (Casal et al., 2001). The samples we studied from this deposit, labelled VAL and VIC, have BET surface values of 308 and 217 m^2g^{-1}, respectively. There are very few data describing the area of microporous sepiolite, but those referred by Galán (1985) for sepiolite from Vallecas are in accordance with that found in this study (Table 3). Galán (1985) found values of 139 $m^2g^{-1}$and 145 m^2g^{-1} for the external- and microporous surfaces, respectively. Sepiolites from other deposits near Vallecas-Vicálvaro, which are also found in the Tajo Basin, are named as BAT and YUN and have been studied by other authors and like in the previous examples, different values have been reported. The values of BET surface of these two samples (Table 3) are 322 m^2g^{-1} and 295 m^2g^{-1}, while those referring to these samples in bibliography are 220 m^2g^{-1} (Legido et al., 2007) and between 330 and 340 m^2g^{-1} (Casal et al., 2001; Molina-Sabio et al., 2001, and Ruiz Hitzky, 2001).

As previously discussed, there are important differences in the results obtained by different authors studying sepiolites coming from the same deposits. These differences can be caused both by the textural variability of natural samples and by the differences in the processes of their preparation and the study of the samples. The texture and microtexture of the samples are the result of the environmental conditions for formation and growth and they are characteristic of each deposit. The textural differences in a deposit are generally not too big. When there are varieties in a deposit, as a result of temporary or spatial changes in its formation conditions, then these varieties are studied as different materials like in Ünal and Erdogan (1998) for the Polatli deposit previously referred. In most cases, the discrepancy in the values obtained studying the "same" samples are the result of different pre-treatments of the samples. Natural samples can be powered by hand or mechanical mortars, dispersed in water, heated or even "cleaned" by soft acid treatment. All of these procedures affect the texture of the samples and influence in the final data recorded. The process of powdering changes the texture of the particles and the final value of the SSA can vary. For example, sepiolite from Korea doubles its surface after grinding (Nishimura et al., 1972), and the SSA of the sepiolite from Las Cruces (Nevada) can vary between 172 and 286 m^2g^{-1} depending on the length of time used for grinding (Bastida et al., 2006). In addition, conditions of out-gassing in the adsorption studies are also very different. Grillet

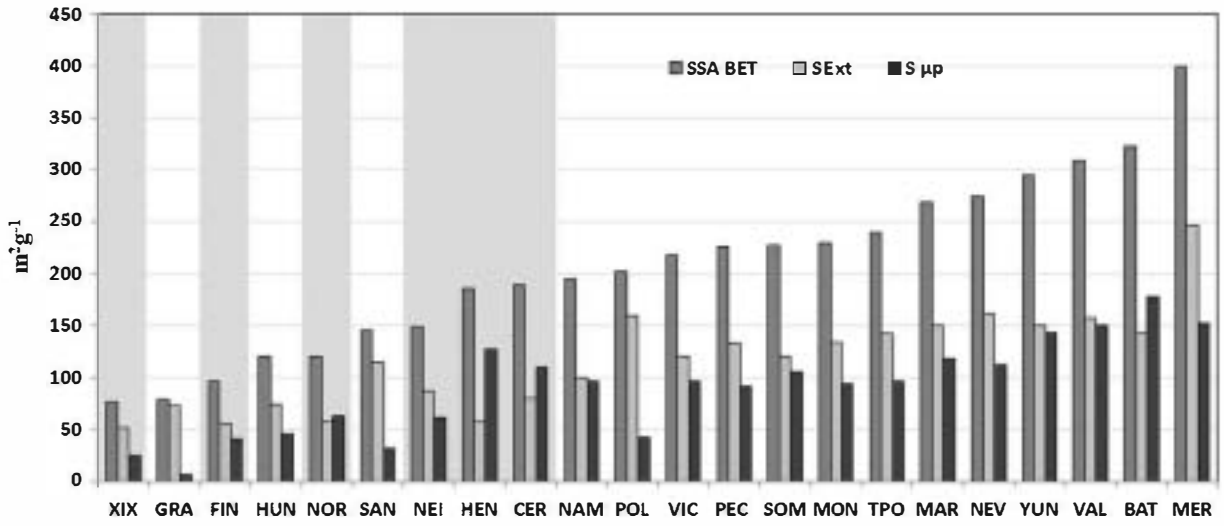

Fig. 6. Graphical representation of the SSA_{BET}, SSA_{Ext} and of the samples $SSA_{\mu p}$. The samples are ordered from the lowest to the highest values of BET. Samples with a grey shadow are macroscopics.

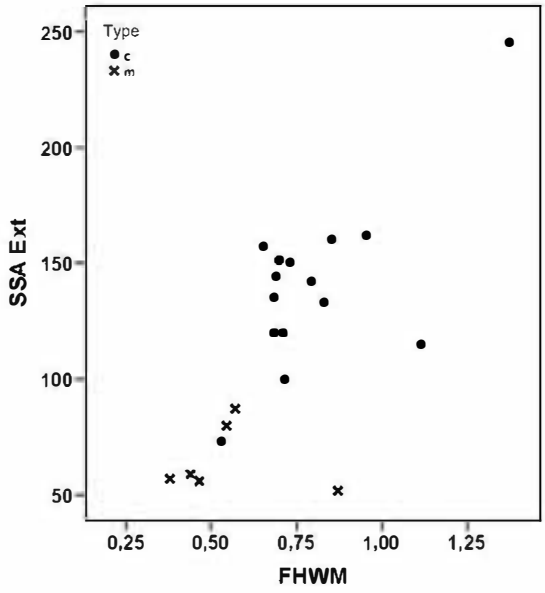

Fig. 7. SSA_{Ext} in m^2g^{-1} versus $FHWM_{110}$ in degrees of 2Θ for macroscopic (black circle) and clay sepiolites (crosses).

et al. (1988) studied the influence of the final out-gassing temperature in the S_{BET} of micronised sepiolite from Vallecas and they found that it can vary between 364 and 120 m^2g^{-1} in the interval of out-gassing temperatures from 25 °C to 500 °C.

In this study, all of the samples have been pre-treated and analysed using the same conditions and, therefore, the results obtained are comparable with one another. One of the factors to take into consideration is the purity of the sample. If there are other minerals with lower values of SSA in the sample, they have an influence on the total value obtained. Most samples investigated in this study are pure, without traces of other minerals in the XRD patterns. Only some of the samples studied contain small amounts of impurities, generally quartz and magnesic minerals, like talc and carbonates (Table 1). Additionally, traces of palygorskite have been detected in three samples. Taking into account that the main impurities do not contribute to the surface, the values obtained for samples with impurities can be extrapolated to 100% of sepiolite. The calculated SSA_{BET} of these samples increases using this assumption, but the general trends are the same. In addition, because the samples with the lowest SSA_{BET} are very pure (XIX and GRA), the content of impurities cannot be argued to be a main factor influencing the differences observed.

There is only a type of impurity that is difficult to be detected by XRD and this can have a great influence on the SSA. Small amounts of amorphous silica are not detected by XRD but could influence the inaccessibility of N_2 along of the structural channels if this silica covers the fibres and closes the entrance of the pores. This could be one of the explanations for the GRA, SAN and XIX samples having the lowest micropore areas. Most samples investigated in this study had been studied previously from the point of view of the crystallochemistry in Garcia-Romero and Suarez (2010) and the presence of amorphous silica has been already been considered to explain the excess of Si in these samples (GRA, SAN and XIX).

The presence of small amounts of impurities does not greatly influence the surface properties but the most extreme values of these properties previously referred to correspond to very pure samples. Therefore, the variations have to be explained from the specific features of each sample. The high values of the SSA of this mineral are related to its fibrous morphology and small particle size, and especially with the structural channels (or tunnels) that characterise this mineral. Taking into account these considerations, the results of the SSA should be similar for all of the studied samples because all of them are sepiolite, which implies the presence of channels. Only small variations should be found and related to the length of the fibres. The discrepancy in the results obtained (Table 3) has to be explained from the specific features of each sample.

As can be seen in Fig. 6, all macroscopic sepiolites are located in the region of the plot corresponding to the lower values of SSA_{BET}, although two clay sepiolites (GRA and HUN) are also among those which have the lowest values. Although there are common

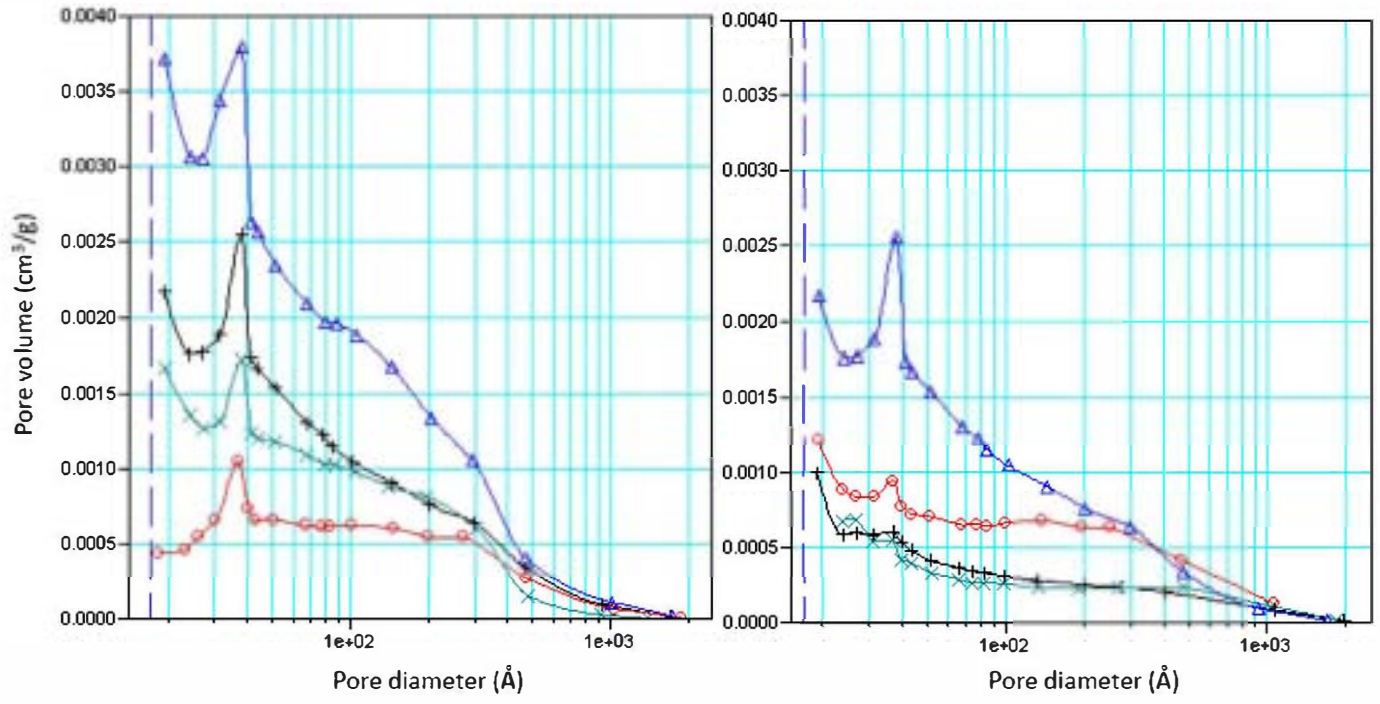

Fig. 8. Distribution of pores. Left: representative clay sepiolites, GRA, SOM, VAL and MER and right: macroscopic sepiolites NOR, HEN, CER and VAL for comparison (from the bottom to the top).

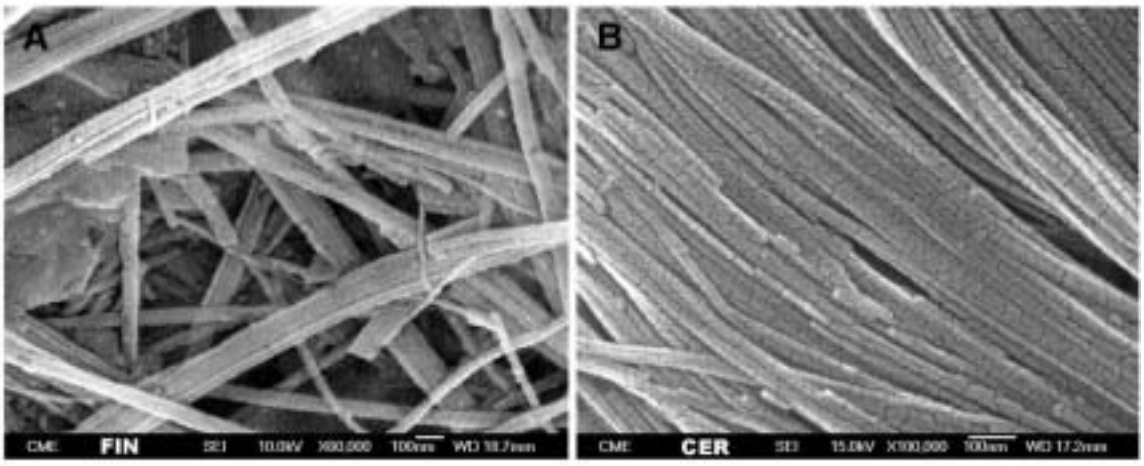

Fig. 9. Two macroscopic sepiolites (FIN and CER) showing very different porosity related to the arrangement of the crystal. A: open porosity without textural microporosity. B: closed porosity and textural interfibre microporosity.

characteristics among all of the macroscopic samples, it is not possible to say that this is a determinant factor in the surface properties. In general, macroscopic sepiolites have lower values of SSA_{BET}, but microporosity is not related to the size of the fibre.

If the surface of sepiolite is mainly related to its structural microporosity, then 1) all of the samples belonging to the same type, macroscopic and clay, should have similar values of SSA_{BET} and similar microporous surface area (MPA), and 2) the presence of impurities has a great influence on the final value of MPA. The macroscopic sepiolites could have lower N_2 accessibility along the tunnels and, as a consequence, lower values of MPA than clay sepiolites. However, macroscopic sepiolites like CER or HEN, the latter presenting fibres centimetres long (Fig. 1), have high values of microporosity, similar or higher than that of some clay sepiolites with much smaller length of fibres. Thus, accessibility of N_2 in the channels may not be a problem.

Another factor to take into account to explain the differences in the N_2 accessibility along the structural channels is the crystallinity of the samples. Crystalline defects can have an influence by either decreasing or increasing the microporosity. If there are defects in the staking of the ribbons in the [100] or the [010] directions, they could produce discontinuity in the channels in the [001] direction causing *closed regions* along the fibre. In this case, bad crystallinity causes a decrease of the obtained values compared to the expected values. On the contrary, a greater micro- or mesoporosity could be obtained if there are defects related to the omission of one or more of the ribbons or polysomes in the inner of the crystal, like those showed by Raoutureau and Tchoubard (1976). These types of defects have been recently described by Krekeler and Guggenheim (2008), and they have been named *open channel defects (OCP)*. In this case micro- or mesoporosity could depend on the size of the OCPs. Ruiz Hitzky (2001) explained the presence of open pores (>15 Å) in a sample after folding by the existence of crystalline defects.

Although the presence of one or both types of defects is difficult to evaluate, the global crystallinity of the samples can be estimated from the XRD data. Hibino et al. (1995) compared five sepiolite samples from different deposits and concluded that the differences found in the SSA_{BET} of those samples were related to the FHWM of the 110 reflection, and therefore related to the crystallinity. In our samples, the correlations among the $FHWM_{110}$, used as a crystallinity index, and data of adsorption are: i) BET surface cc = 0.490, ii) External surface cc = 0.731 and iii) Micropore area cc = 0.130. From these data and that which is shown in Fig. 7, there is a relation between $FHWM_{110}$ and the external surface calculated from the isotherms. In this figure, the grouping of the macroscopic sepiolites falls in the region of lower external surfaces and better crystallinity. The external surface depends on the size of the fibres and in the macroscopic samples, the fibres are larger. In addition, well developed crystals are a result of stable physicochemical conditions during their growth. On the contrary, both the volume of pores and the micropore area have no relation to the FHWM values obtained.

The high variability in the values of the microporosity, both for the micropore area and volumes, cannot be explained by considering the

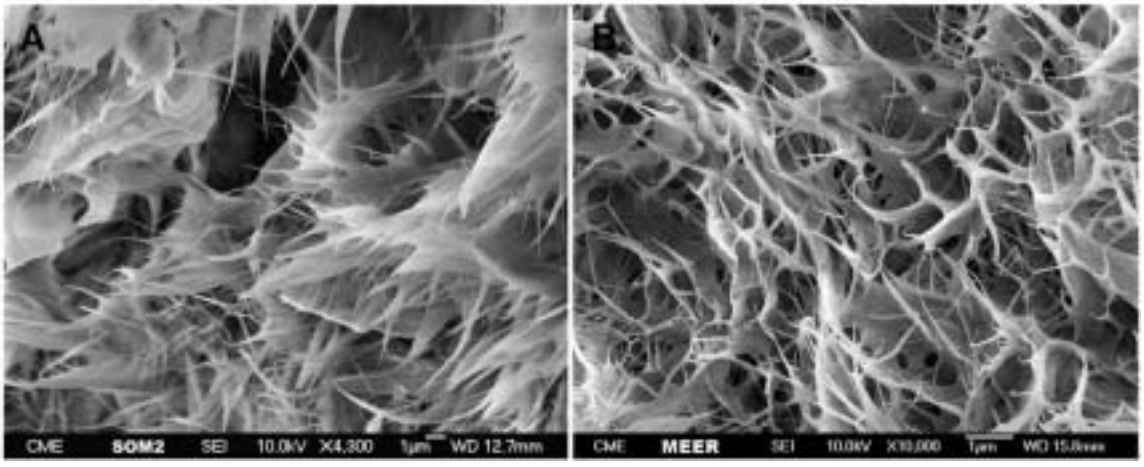

Fig. 10. SOM and MER samples showing their characteristic texture, different to the others sepiolites.

differences in the length of the fibre or by the accessibility of the structural tunnels. Only differences in the length of the tunnels, a consequence of the length of fibres, could be argued. However, as discussed previously, there is no relationship between length and microporosity. As can be seen in Fig. 8, the distribution of micro- and mesoporosity is very different. In this figure, representative samples are shown, arranged from highest to lowest SSA_{BET} values. In the region under 30 Å, all of the samples present a characteristic peak related to the entrance of N_2 inside the intracrystalline tunnels. All of the samples present this peak, but the volume of the pores per gram of this size of pores is lower in the macroscopic samples. This observation reveals the fact that there is a problem of accessibility of the N_2 along the pores in the longer fibres.

Besides the structural microporosity that characterise sepiolite, an *interfibre microporosity* can be described. This textural microporosity is dependent on the arrangement of the fibres and, therefore, each sample has its own characteristic features. For this reason, in the region under 30 Å, there are differences among the samples as shown in Fig. 8. Fig. 9 shows two macroscopic samples, FIN and CER, which have $SSA_{\mu p}$ values of 41 and 110 m^2g^{-1}, respectively. The microtexture of these samples is very different. FIN has very separated fibres with an open porosity while CER shows parallel fibres with interfibre microporosity; these differences can be related to the data of surface recorded showing the relationship between microporosity and texture.

Finally, the influence of texture is also easy to deduce when comparing samples like SOM and MER. Fig. 10 displays how these samples present a very similar texture, but differing values of SSA_{BET}. SOM presents one of the lowest amounts of sepiolite among the studied samples and has more than 100 m^2g^{-1} of $SSA_{\mu p}$. If the value of SSA_{BET} is extrapolated to 100% of sepiolite, the external surface and the surface of micropores would be the highest of this collection of sepiolites, after those values obtained for MER sample.

5. Final remarks

From the data reported above, the following conclusions can be drawn:

1. There is a great variability in the surface properties in natural sepiolites. The exceptionally low values of these properties found in some samples cannot be related to the presence of impurities, but rather to their structural and textural features.
2. The surface properties of sepiolite are not only related to its structural microporosity since the texture is a determining factor influencing the final values of the SSA. Two types of microporosity can be described: *structural microporosity* and *interfibre microporosity*.
3. Other characteristics of the individual crystals, like the length of the fibres and the crystallinity, also influence the surface properties. The accessibility of N_2 to the intracrystalline tunnels is higher for the shorter fibres.
4. The SSA and the porosity of each sepiolite are the result of the sum of the intracrystalline or structural microporosity and the textural porosity (interfibre microporosity and mesoporosity). As a consequence, there is a hierarchical distribution of pore sizes (Fig. 11) which is different for each sepiolite.
5. Sepiolites with a higher SSA are those that have a smaller length and a more closed porosity.

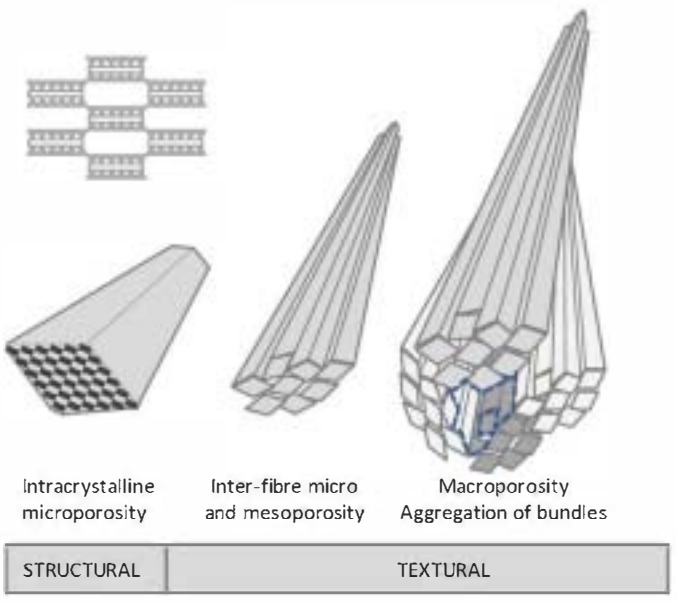

Fig. 11. Schematic representation of the hierarchical distribution of pores in sepiolite, from the intracrystalline and structural microporosity, to the textural mesoporosity caused by the aggregation of bundles of fibres.

Acknowledgement

The authors are grateful to Tolsa and MYTA for supplying some samples. Financial support was provided by CICYT (CGL2009-10764).

References

Alkan, M., Demirbas, O., Dogan, M., 2007. Adsorption kinetics and thermodynamics of an anionic dye onto sepiolite. Microporous and Mesoporous Materials 101, 388–396.

Álvarez, A., Santarém, J., Esteban-Cubillo, A., Aparicio, P., 2011. Current industrial applications of palygorskite and sepiolite. Ch 12. In: Galán, E., Singer, A. (Eds.), Developments in Palygorskite–Sepiolite Research. A New Look at These Materials. Elsevier, Amsterdam.

Balci, S., 1999. Effect of heating and acid pre-treatment on pore size distribution of sepiolite. Clay Minerals 34, 647–655.

Bastida, J., Kojdecki, M.A., Pardo, P., Amorós, P., 2006. X-ray diffraction line broadening on vibrating dry-milled Two Crows sepiolite. Clays and Clay Minerals 54–3, 390–401.

Brauner, K., Presinger, A., 1956. Struktur und Entstehung des Sepioliths. Tschermak's Mineralogische und Petrographische Mitteilungen 6 (1–2), 120–140.

Brunauer, S., Emmet, P.H., Teller, E., 1936. Adsorption of gases in multimolecular layers. Journal of the American Chemical Society 60, 309–319.

Campelo, J.M., García, A., Luna, D., Marinas, J.M., 1987. Surface properties of sepiolites from Vallecas-Madrid, Spain, and their catalytic activity in cyclohexene skeletal isomerisation. Reactivity of Solids 3, 263–272.

Casal, B., Merino, J., Serratosa, J.M., Ruiz-Hitzky, E., 2001. Sepiolite-based materials for the photo- and thermal-stabilization of pesticides. Applied Clay Science 18, 245–254.

Chen, H., Zeng, D., Xiao, X., Zheng, M., Ke, C., Li, Y., 2011. Influence of organic modification on the structure and properties of polyurethane/sepiolite nanocomposites. Materials Science and Engineering A 528, 1656–1661.

Chryssikos, G.D., Gionis, V., Kacandes, G.H., Stathopoulou, E.T., Suárez, M., García-Romero, E., Sánchez del Rio, M., 2009. Octahedral cation analysis of palygorskite by near-infrared spectroscopy. American Mineralogist 94, 200–203.

Cornejo, J., Hermosín, M.C., 1988. Structural alteration of sepiolite by dry grinding. Clay Minerals 23, 391–398.

Dandy, A.J., Nadiye-Tabbiruka, M.S., 1982. Surface properties of sepiolite from Amboselo, Tanzania, and its catalytic activity for ethanol decomposition. Clays and Clay Minerals 30, 347–352.

De Boer, J.H., Lippens, B.C., 1964. Studies on pore systems in catalysts II. The shapes of pores in aluminum oxide systems. Journal of Catalysis 3, 38–43.

del Hoyo, C., Dorado, D., Rodríguez-Cruz, M.-S., Sánchez-Martín, M.J., 2008. Physicochemical study of selected surfactant-clay mineral system. Journal of Thermal Analysis and Calorimetry 91, 227–234.

Frost, R.L., Ding, Z., 2003. Controlled rate thermal analysis and differential scanning calorimetry of sepiolites and palygorskites. Thermochimica Acta 397, 119–128.

Galán, E., 1985. Industrial applications of sepiolite from Vallecas-Vicalvaro, Spain: a review. In: Schulltz, L.G., van Olphen, H., Mumpton, F.A. (Eds.), Proc. International Clay Conference. Denver, 1985. The Clay Mineralogical Society, Bloomington, Indiana, pp. 400–404.

Galán, E., Aparicio, P., Miras, A., 2011. Sepiolite and palygorskite sealing materials for geological storage of carbon dioxide. Ch 16. In: Galán, E., Singer, A. (Eds.), Developments in Palygorskite-Sepiolite Research. A New Look at These Materials, Elsevier, Amsterdam.

Garcia-Romero, E., Suarez, M., 2010. On the chemical composition of sepiolite and palygorskite. Clays and Clay Minerals 58, 1–20.

García-Romero, E., Suárez, M., Santarén, J., Álvarez, A., 2007. Crystallochemical characterization of the palygorskite and sepiolite from the Allou Kagne deposit, Senegal. Clays and Clay Minerals 6, 606–617.

Gómez-Avilés, A., Darder, M., Aranda, P., Ruiz-Hitzky, E., 2010. Multifuncional materials based on graphene-like/sepiolite nanocomposites. Applied Clay Science 47, 203–211.

Grillet, Y., Cases, J.M., Francois, M., Rouquerol, J., Poirier, J.E., 1988. Modification of the porous structure and surface area of sepiolite. Clays and Clay Minerals 36, 233–242.

Güngör, N., Isçi, S., Günisten, E., Mista, W., Teteryez, H., Klimkiewickz, R., 2006. Characterization of sepiolite as a support of silver catalyst in soot combustion. Applied Clay Science 32, 291–296.

Hibino, T., Tsunashima, A., Yamazaki, A., Otsuka, R., 1995. Model calculation of sepiolite surface areas. Clays and Clay Minerals 43, 91–396.

Inagaki, S., Fukushima, Y., Doi, H., Kamigaito, O., 1990. Pore distribution and adsorption selectivity of sepiolite. Clay Minerals 25, 99–105.

Jia, Q.M., Shan, S.Y., Jiang, L.H., Wang, Y.M., 2010. Synthesis and properties epoxy resin/mesoporous silica-sepiolite nanocomposites. Advanced Materials Research 129–131, 1248–1251.

Krekeler, M.P.S., Guggenheim, S., 2008. Defects in microstructure in palygorskite–sepiolite minerals: a transmission electron microscopy (TEM) study. Applied Clay Science 39, 98–105.

Kuang, U., Facey, G.A., Detellier, C., 2006. Organo-mineral nanohybrids. Incorporation, coordination and structuration role of acetone molecules in the tunnels of sepiolite. Journal of Materials Chemistry 12, 179–185.

Iegido, J.L., Medina, C., Mourelle, M.L., Carretero, M.I., Pozo, M., 2007. Comparative study of the cooling rates of bentonite, sepiolite and common clay for their use in pelotherapy. Applied Clay Science 36, 148–160.

Mehmet, U., 2009. Adsorption of a textile dye onto activated sepiolite. Microporous and Mesoporous Materials 119, 276–283.

Molina-Sabio, M., Caturla, F., Rodriguez-Reinoso, F., Kharitonova, G.V., 2001. Porous structure of a sepiolite as deduced from the adsorption of N_2, CO_2, NH_3 and H_2O. Microporous and Mesoporous Materials 47, 389–396.

Murray, H.H., 1999. Applied clay mineralogy today and tomorrow. Clay Minerals 34, 39–49.

Nishimura, Y., Hori, Y., Takahashi, H., 1972. Structural change and adsorption character of sepiolite by heat treatment. Journal of the Clay Science Society of Japan 12, 102–108.

Özdemir, O., Cinar, M., Sabah, E., Arslan, F., Celik, M.S., 2007. Adsorption of anionic surfactants onto sepiolite. Journal of Hazardous Materials 147, 625–632.

Post, J.E., Bish, D.L., Heaney, P.J., 2007. Synchrotron powder X-ray diffraction study of the structure and dehydration behavior of sepiolite. American Mineralogist 92, 91–97.

Raoutureau, M., Tchoubard, C., 1976. Structural analysis of sepiolite by selected area electron diffraction-relation with physico-chemical properties. Clays and Clay Minerals 24, 43–49.

Rautureau, M., Mifsud, A., 1977. Ètude par microscopie electronique des different etats d'hydration de la sepiolite. Clay Minerals 77, 309–318.

Ruiz Hitzky, E., 2001. Molecular access to intracrystalline tunnels of sepiolite. Journal of Materials Chemistry 11, 86–91.

Ruiz Hitzky, E., Aranda, P., Álvarez, A., Santarém, J., Esteban-Cubillo, A., 2011. Advanced materials and new applications of sepiolite and palygorskite. Ch 17. In: Galán, E., Singer, A. (Eds.), Developments in Palygorskite–Sepiolite Research. A New Look at These Materials. Elsevier, Amsterdam.

Sánchez del Río, M., García-Romero, E., Suárez, M., da Silva, I., Fuentes Moreno, L., Martín-Criado, G., 2011. Variability in sepiolite. American Mineralogist 96, 1443–1454.

Sánchez-Martín, M.J., Rodríguez-Cruz, M.S., Andrades, M.S., Sánchez-Camazano, M., 2006. Efficiency of different clay minerals modified with a cationic surfactant in the adsorption of pesticides: influence of clay type and pesticide hydrophobicity. Applied Clay Science 31, 216–228.

Schultz, L.G., 1964. Quantitative interpretation of mineralogical composition from X-ray and chemical data for the Pierre Shale. U.S. Geological Survey Professional Paper 391-C, 1–31.

Serna, C., van Scoyoc, G.E., 1979. Infrared study of sepiolite and palygorskite surfaces. In: Mortland, M.M., Farmer, V.C. (Eds.), Proceedings International Clay Conference 1978. Elsevier, Amsterdam, pp. 197–206.

Serna, C., Ahlrichs, J.L., Serratosa, J.M., 1975. Folding in sepiolite crystals. Clays and Clay Minerals 23, 452–457.

Shuali, U., Nir, S., Rytwo, G., 2011. Adsorption of surfactants, dyes and cationic herbicides on sepiolite and palygorskite: modifications, applications and modelling. Ch 15. In: Galán, E., Singer, A. (Eds.), Developments in Palygorskite-Sepiolite Research. A New Look at These Materials, Elsevier, Amsterdam.

Stathopoulou, E.T., Suarez, M., Garcia-Romero, E., Sanchez del Rio, M., Kacandes, G.H., Gionis, V., Chryssikos, G.D., 2011. Trioctahedral entities in palygorskite: near-infrared evidence for sepiolite-palygorskite polysomatism. European Journal of Mineralogy 23, 567–576.

Suárez, M., García-Romero, E., 2011. Advances in the crystal chemistry of sepioite and palygorskite. Ch 2. In: Galán, E., Singer, A. (Eds.), Developments in Palygorskite–Sepiolite Research. A New Look at These Materials. Elsevier, Amsterdam.

Türker, A.R., Bag, H., Erdogan, B., 1997. Determination of iron and lead by flame atomic absorption spectrometry after preconcentration with sepiolite. Fresnius´ Journal of Analytical Chemistry 357, 351–353.

Ünal, H.I., Erdogan, B., 1998. The use of sepiolite for decolorization of sugar juice. Applied Clay Science 12, 419–429.

Viseras, C., Aguzzi, C., Cerezo, P., Bedmar, M.C., 2008. Biopolymer-clay nanocomposites for controlled drug delivery. Materials Science and Technology 29, 1020–1026.

Zheng, S.Q., Han, Y., Huang, X.H., Dai, Y.L., Qian, D., Hang, J.C., Ren, S., 2010. Acid and aluminium modification of sepiolite and its application in FCC catalysis. Clay Minerals 45, 15–22.